

## Thermomechanical noise of a free v-shaped cantilever for atomic force microscopy

Robert W. Stark, Tanja Drobek, and Wolfgang M. Heckl

*Universität München,  
Institut für Kristallographie und Angewandte Mineralogie,  
Theresienstr. 41,  
80333 München, Germany  
phone: ++49-89-23944340,  
fax: ++49-89-23944331  
e-mail: robert@nanomanipulation.de*

(Dated: May 27, 2000)

We have calculated the thermal noise of a v-shaped AFM cantilever (Microlever, Type E, Thermomicroscopes) by means of a finite element analysis. The modal shapes of the first ten eigenmodes are displayed as well as the numerical constants which are needed for a calibration using the thermal noise method. In the first eigenmode, values for the thermomechanical noise of the z-displacement at 22° C temperature of  $\sqrt{\langle u_n^2 \rangle} = 0.627 \text{ \AA} / \sqrt{c_{\text{cant}}}$  and the normal force photodiode signal of  $\sqrt{\langle S_n^2 \rangle} = 0.558 \text{ \AA} / \sqrt{c_{\text{cant}}}$  were obtained. The results also indicate a systematic deviation of the spectral density of the thermomechanical noise of v-shaped cantilevers as compared to rectangular beam shaped cantilevers.

keyword: atomic force microscopy

PACS 96: 61.16Ch, 07.79Lh, 07.10Cm, 43.40Hb

### I. INTRODUCTION

The micromechanical cantilevers commonly used in atomic force microscopy (AFM) are forced to non-negligible thermomechanical oscillations already at room temperature. These oscillations impose a fundamental restriction to the accuracy of force detection in AFM [1–3]. A similar limit of sensitivity in force detection is encountered in experimental setups for the detection of gravitational waves (e.g. [4] and references therein). However, the thermally driven oscillations can be analyzed in order to obtain information on the tip-sample interaction. It was shown, that thermomechanical noise allows for the determination of oscillatory hydration potentials [5] as well as the measurement of viscoelastic properties of polymers [6, 7].

Another very common application of thermomechanical noise analysis is the fast and nondestructive calibration of the cantilever spring constant [8–13]. Present theoretic descriptions of thermomechanically induced noise in AFM measurements assume a rectangular geometry of the cantilever [10, 14, 15].

In practical AFM applications, very often v-shaped cantilevers are used as force sensors, for example in the magnetically driven intermittent contact mode [16, 17]. Moreover, there are several applications in the different operational modes of overtone microscopy, where v-

shaped cantilevers are commonly employed [18–20]. For all applications of v-shaped cantilevers in dynamic AFM modes the calibration of the spring constant and the exact knowledge of the eigenmodes are essential prerequisites for a quantitative data analysis. This is also true for nanomanipulation experiments (e.g. [21, 22]) or the use of cantilevers as chemical sensors (e.g. [23]).

In this paper, a v-shaped cantilever is investigated theoretically by means of a finite element analysis (FEA). The results of the numerical simulations are used in order to determine the thermomechanical noise of the tip z-displacement and the photodiode signal of the unrestricted cantilever which allows to calculate a calibration table for the determination of the cantilever spring by the thermal noise method. Using a discrete numerical method like FEA it is possible to calculate the thermal oscillations for arbitrary cantilever geometries.

### II. OUTLINE OF THEORY

#### A Thermomechanical noise

In thermodynamic equilibrium the mean-square displacement of the tip from its neutral position is described

by

$$\sqrt{\langle u^2 \rangle} = \sqrt{\frac{k_B T}{c_{\text{cant}}}}. \quad (1)$$

Here,  $u$  is the  $z$ -displacement of the tip,  $k_B$  is Boltzmann's constant,  $T$  the temperature of the surrounding heat bath,  $c_{\text{cant}}$  the cantilever spring constant, and  $\langle \cdot \rangle$  denotes the average in time (cf. e.g. [8]). Note that this formula is independent from the cantilever geometry.

However, when light-lever detection is used for the displacement measurement, experimental noise-data cannot be analyzed applying Equation (1). In order to calculate the photodiode signal in a light-lever setup, the shape of the transverse vibrational modes must be known to correct for geometric effects. Equation (1) has to be corrected for the bandwidth limitation of the detection system as well.

## B Multiple degrees of freedom

For a mathematical description of the cantilever dynamics in a frequency range above the fundamental frequency the cantilever must be modelled as a multiple-degree of freedom system. In the following, only a brief review of the basic ideas is given, a more thorough treatment can be found in textbooks on structural dynamics (e.g. [24, 25]).

A discrete finite element approach is used in order to describe a cantilever with arbitrary geometry. In the matrix formalism, the equation of motion is

$$\mathbf{M} \ddot{\mathbf{u}}(t) + \mathbf{K} \mathbf{u}(t) = \mathbf{0}. \quad (2)$$

Here,  $\mathbf{M}$  is the mass matrix,  $\mathbf{K}$  the stiffness matrix, and  $\mathbf{u}(t)$  is the vector of the nodal displacements. The eigenvalue problem is solved in order to determine the resonance frequencies and the eigenmodes of the undamped structure. This yields the eigenvectors  $\Phi_n$  and the eigenfrequencies  $\omega_n$ . The eigenmodes can be used as base vectors of a generalized coordinate system, where it is possible to separate the time and space dependence of the cantilever motion.

For the transformation into generalized displacement coordinates  $q_n(t)$  the transformation rule

$$\mathbf{u}(t) = \sum_n \Phi_n q_n(t) \quad (3)$$

is applied to Equation (2), yielding

$$\sum_n [\mathbf{M} \Phi_n \ddot{q}_n(t) + \mathbf{K} \Phi_n q_n(t)] = \mathbf{0}. \quad (4)$$

Multiplication with  $\Phi_n^T$  results in

$$\sum_n [\Phi_n^T \mathbf{M} \Phi_n \ddot{q}_n(t) + \Phi_n^T \mathbf{K} \Phi_n q_n(t)] = \mathbf{0}. \quad (5)$$

This leads to the definition of  $M_n = \Phi_n^T \mathbf{M} \Phi_n$  as the generalized mass and  $K_n = \Phi_n^T \mathbf{K} \Phi_n$  as the generalized spring stiffness. Now, a set of decoupled ordinary differential equations

$$M_n \ddot{q}_n(t) + K_n q_n(t) = 0 \quad (6)$$

is obtained.

In the case of a constant mass density of the structure and orthonormal  $\Phi_n$ , the generalized mass equals the total mass:

$$M_n = \Phi_n^T \mathbf{M} \Phi_n = M. \quad (7)$$

The generalized spring stiffness is then

$$K_n = M \omega_n^2. \quad (8)$$

Treating the cantilever as a system of  $N$  harmonic oscillators in thermodynamic equilibrium, the mean-square displacement of the individual generalized oscillators is given by

$$\langle q_n^2 \rangle = \frac{k_B T}{K_n}. \quad (9)$$

Note that the  $K_n$  are not equal to the (quasistatic) spring constant  $c_{\text{cant}}$ .

The average potential energy of the cantilever in thermal equilibrium is given by

$$\langle U_{\text{cant}} \rangle = \frac{1}{2} c_{\text{cant}} \langle u^2 \rangle = \frac{1}{2} k_B T. \quad (10)$$

The fraction of average potential energy of the  $j$ -th node of the cantilever found in the  $n$ -th eigenmode can be determined from

$$C_{n,j} = \Phi_{n,j}^2 / \frac{K_n}{c_{\text{cant}}}, \quad (11)$$

The quasistatic spring constant  $c_{\text{cant}}$  is determined by a static structural analysis. For the calculation of tip displacement a node  $j$  is chosen at the tip. The value  $C_{n,j}$  represents the percentage of energy of the multiple degree of freedom system found in the  $n$ -th eigenmode.

It is worth to note that other generalized coordinate systems could be used as well. Often the effective mass  $m^*$  is used in order to describe the dynamics of a vibrating cantilever. This corresponds to a coordinate system which is different from the system we apply here. Still another coordinate system is often used in commercial finite element software. There, the  $\Phi_n$  are normalized by the condition  $\hat{\Phi}_n^T \mathbf{M} \hat{\Phi}_n = 1$  (e.g. [26]). Equation (11) in this third type of coordinate system transforms into  $C_{n,j} = \frac{\hat{\Phi}_{n,j}^2}{m} / \frac{K_n}{c_{\text{cant}}} = \hat{\Phi}_{n,j}^2 / \frac{\omega_n^2}{c_{\text{cant}}}$ . However, since the choice of the generalized coordinate system is arbitrary, identical numerical results are obtained. A more detailed treatment can be found in Ref. [27].

In order to account for the light-lever detection scheme, another correction factor has to be introduced:

$$C_{n,j}^{\text{det}} = \left[ \frac{\partial_x \Phi_{n,j}}{\partial_x \Psi_j} \right]^2. \quad (12)$$

This factor represents the relation of the geometrical derivative of the quasistatic bending shape  $\partial_x \Psi_j$  to the dynamic bending shape  $\partial_x \Phi_{n,j}$  of the  $n$ -th eigenmode and can be understood as a geometric enhancement factor. For eigenmodes with  $C_{n,j}^{\text{det}} > 1$ , the photodiode signal is increased, whereas when  $C_{n,j}^{\text{det}} < 1$  the photodiode signal is decreased as compared to the photodiode signal of a quasistatic cantilever deflection.

Both parameters  $C_{n,j}$ , and  $C_{n,j}^{\text{det}}$  are independent from the material parameters, mass density  $\rho$  and the Young's Modulus  $E$ , since they enter as linear factors into the mass or stiffness matrix and can therefore be cancelled.

### C Spectral power density

For a general continuous multimode system, the spectral power density was given in Ref. [4]. A detailed discussion for rectangular AFM cantilevers can be found in [14]. In a similar approach, the displacement of the  $j$ -th node in the  $n$ -th mode for a discrete multiple-degree of freedom system is obtained by

$$\langle u_n^2(\omega) \rangle_j = \Phi_{n,j}^2 \frac{2k_{\text{B}}T}{m} \frac{\gamma_n/m}{(\omega_n^2 - \omega^2)^2 + (\omega \gamma_n/m)^2}, \quad (13)$$

and the root-mean square photodiode signal measured at node  $j$  is

$$\langle S_n^2(\omega) \rangle_j = C_{n,j}^{\text{det}} \Phi_{n,j}^2 \frac{2k_{\text{B}}T}{m} \frac{\gamma_n/m}{(\omega_n^2 - \omega^2)^2 + (\omega \gamma_n/m)^2}. \quad (14)$$

Often the quality factor  $Q$  is used instead of a damping coefficient  $\gamma_n$ , thus  $\gamma_n/m = \omega_n/Q$  has to be applied then. By integration, the modal thermomechanical deflection and the photodiode signal can be calculated:

$$\langle u_n^2 \rangle_j = \frac{1}{2\pi} \int_{-\infty}^{\infty} \langle u_n^2(\omega) \rangle_j d\omega, \quad (15)$$

$$\langle S_n^2 \rangle_j = \frac{1}{2\pi} \int_{-\infty}^{\infty} \langle S_n^2(\omega) \rangle_j d\omega. \quad (16)$$

With an additionally weighting factor in Equations (15) and (16), the transfer function of the detection system could also be included.

The mean-square of the deflection and the photodiode signal of the  $N$ -oscillator cantilever at node  $j$  is obtained

from

$$\langle u^2 \rangle_j = \sum_{n=1}^N \langle u_n^2 \rangle_j \quad (17)$$

$$\langle S^2 \rangle_j = \sum_{n=1}^N \langle S_n^2 \rangle_j. \quad (18)$$

In the following, the index  $j$  will be suppressed. By convention, we choose a node of the model at the rear side of the cantilever just above the AFM tip as indicated in Figure 1 (a).

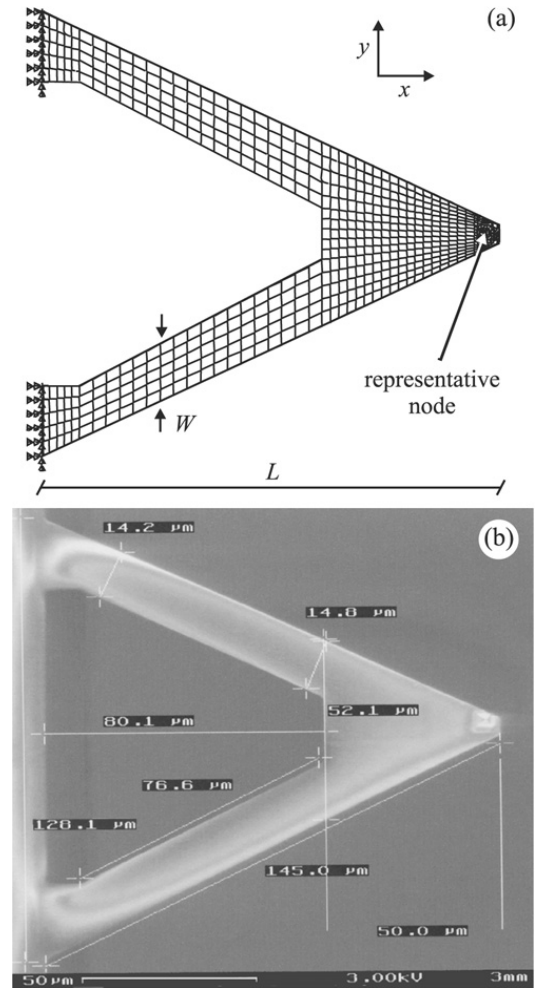


FIG. 1: (a) Mesh of the AFM cantilever used for the finite element analysis (FEA). The arrows at the cantilever base represent the restrictions of the nodal degrees of freedom. The large arrow points at a node which was chosen in order to calculate the nodal deflection. (b) Scanning electron micrograph of the cantilever. The geometric data were used for the FEA as indicated. [Gold coated sharpened microlever, type E, Thermomicroscopes]

### III. RESULTS AND DISCUSSION

In order to obtain precise geometric data for the finite element modelling, a standard cantilever [gold coated sharpened microlever, type E, Thermomicroscopes, Sunnyvale (CA), USA] was analyzed by scanning electron microscopy. The cantilever thickness was determined from an edge-on micrograph (data not shown). A gold film thickness of 60 nm was measured by AFM imaging of an edge prepared by partially removing the gold layer from the cantilever chip. From the electron microscopy and AFM data [Fig. 1 (b)] the finite element mesh was modelled [Fig. 1 (a)] with a length of  $L = 132 \mu\text{m}$ , a width of  $W = 16 \mu\text{m}$ , and a thickness of  $T = 0.63 \mu\text{m}$  (nominal values:  $L = 140 \mu\text{m}$ ,  $W = 18 \mu\text{m}$ ,  $T = 0.6 \mu\text{m}$ ).

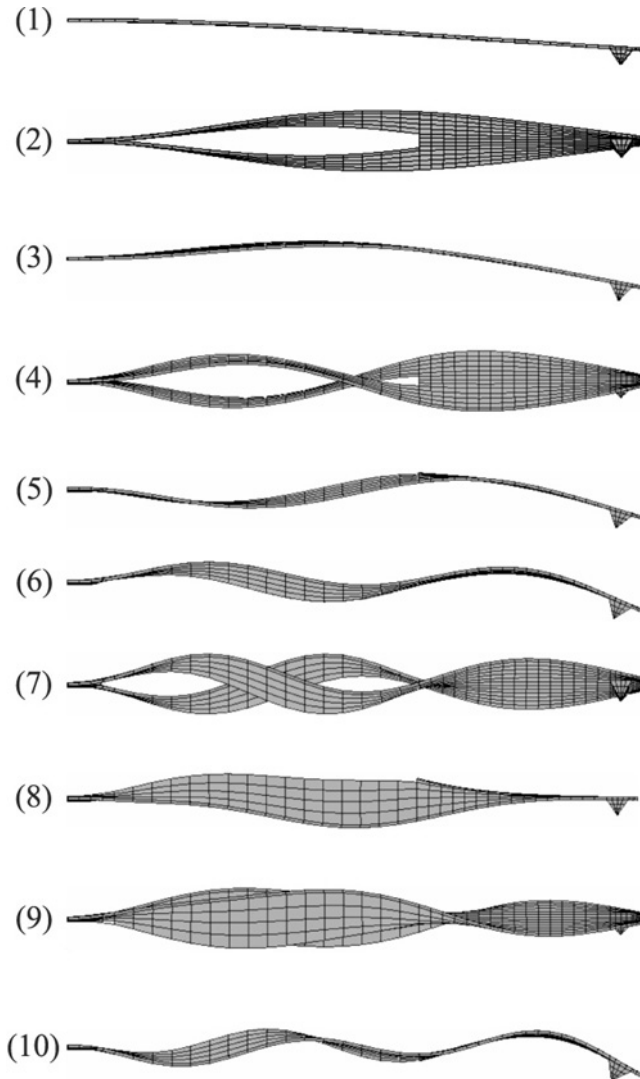


FIG. 2: The first ten eigenmodes of a v-shaped cantilever (sideview). They can be classified into symmetric (1, 3, 5, 6, 8, 10) and antisymmetric (2, 4, 7, 9) modes. Only symmetric modes yield a normal-force photodiode signal.

The finite element analysis (FEA) was carried out by the use of a commercial software ANSYS 5.4 [26] running on an IBM-SP2 workstation at Leibniz Rechenzentrum, München (Germany). The model of the cantilever geometry was built up with brick elements (solid-type 73). A mesh of 2272 nodes was used for the calculations. The mesh independence was demonstrated by further mesh refinement. The silicon nitride/gold system was replaced by a one-component model with the same mass density as the real cantilever. The Young's modulus was set to 140 GPa, therefore the model has the same section moment as the composite cantilever [28]. The Poisson ratio was set to 0.4 in order to reproduce the experimentally obtained resonant frequency ratios of normal and torsional modes. The quasistatic spring constant as obtained from a static FEA is  $c_{\text{cant}} = 0.13 \text{ N/m}$  (manufacturer's value:  $c_{\text{cant}} = 0.10 \text{ N/m}$ ).

mode $n$	frequency	$C_n$	$C_n^{\text{det}}$
1	38.8 kHz	0.963	0.79
2	192.3 kHz	0.000	7.26
3	203.1 kHz	0.036	8.26
4	540.1 kHz	0.000	22.41
5	545.2 kHz	0.004	24.17
6	1054.5 kHz	0.001	60.58
7	1068.7 kHz	0.000	66.55
8	1217.3 kHz	0.001	24.17
9	1507.2 kHz	0.000	56.44
10	1698.3 kHz	0.000	136.45

TABLE I: Summary of cantilever data. The coefficients  $C_n$  give the fraction of energy in the respective mode [cf. Eq. (11)]. Deviations of  $\sum C_n$  from the ideal value of 1.000 are caused by intrinsic numerical errors. The respective geometric amplification of the photodiode signal can be calculated from  $\sqrt{C_n^{\text{det}}}$  [cf. Eq. (12)].

The modal shapes of the first ten transversal eigenmodes obtained by the modal analysis tool [26] are displayed in Figure 2, the respective eigenfrequencies are given in Table I. The eigenmodes can be classified into two categories, symmetric and antisymmetric modal shapes. In the symmetric modes the x-z-plane is a mirror plane, whereas the antisymmetric modes are antisymmetric to the x-direction. From a geometric point of view, some of the symmetric eigenmodes (1, 3, 5, 6, 10) correspond to the first five eigenmodes of a rectangular beam (B1, B2, B3, B4, B5, e.g. [10]) respectively. Note, that in this communication the eigenmodes of a beam are numbered by  $Bn$  in order to avoid confusion with the eigenmodes of the v-shaped cantilever labelled  $n$ . The first three antisymmetric modes (2, 4, 7) correspond to torsional eigenmodes of a rectangular beam. These modes do not contribute to the thermal noise in the z-displacement of the tip, since there the tip oscillates parallel to the sample surface. However, for the eigenmodes (8) and (9) of the v-shaped cantilever there

are no corresponding eigenmodes of a simple rectangular beam. In these modes, both arms of the cantilever vibrate independently from the baseplate. In the symmetric vibration mode (8) both arms vibrate parallel resulting in a motion similar to a bird beating its wings. In the antisymmetric mode (9) both arms twist.

The spectral density of the thermomechanical fluctuations is plotted in Figure 3. The noise in the tip z-deflection decreases much more rapidly with increasing frequency than the noise measured by a light-lever setup (cf. Eqs. 13, 14, summation over  $n$ ). This effect is caused by the geometric enhancement of the higher eigenmodes ( $C_n^{\text{det}} > 1$  for  $n > 1$ ).

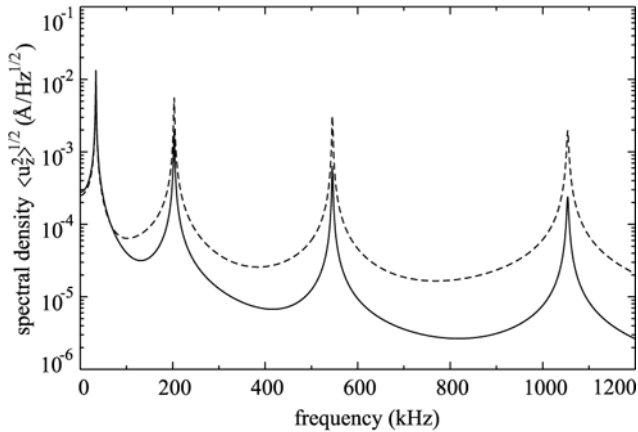


FIG. 3: Spectral density of the thermomechanical fluctuations of the tip-position  $\sqrt{u_z}$  (solid) and the normal-force photodiode signal  $\sqrt{S}$  (dashed) for a resolution bandwidth of 1 Hz.

Table I gives a summary of the eigenfrequencies, the correction factors  $C_n$  and the detection factors  $C_n^{\text{det}}$ . The factors  $C_n$  and  $C_n^{\text{det}}$  are insensitive to deviations in the cantilever geometry. A variation in  $L$  of 10 % causes a relative variation of  $\delta C_n < 2\%$  and  $\delta C_n^{\text{det}} < 3\%$ , whereas the respective eigenfrequencies may vary more than 20 %. Therefore, in comparison to typical experimental errors, there is only a small deviation from the theoretic energy distribution for the thermomechanical noise as derived from Equation (11) due to variations of the cantilever geometry.

Alternatively, the numerical results from Table I can be validated by considering  $\delta U_{\text{num}} = \sum_1^{10} C_n^{\text{eff}} - 1$ , which is the energy "loss" or "gain" of the model due to intrinsic numerical errors. Here, the "energy gain" of the numerical model is  $\delta U_{\text{num}} \approx 0.5\%$ . This means, that the numerical errors in the energy distribution among the eigenmodes can be estimated to be smaller than 1 %.

Table II summarizes the normalized thermomechanical deflection of the tip in z-direction attributed to the different eigenmodes. For comparison, also the values for a rectangular cantilever beam are given for geometrically equivalent eigenmodes (same number of nodes).

mode	beam <sup>a</sup>	mode	v-shape
B1	0.629 Å	1	0.627 Å
–	–	2	0.000 Å
B2	0.100 Å	3	0.121 Å
–	–	4	0.000 Å
B3	0.036 Å	5	0.042 Å
B4	0.018 Å	6	0.021 Å
–	–	7	0.000 Å
–	–	8	0.019 Å
–	–	9	0.000 Å
B5	0.011 Å	10	0.012 Å

TABLE II: Thermomechanical noise of the tip deflection  $\sqrt{\langle u_n^2 \rangle}$  of a beam like [10] and a v-shaped cantilever at 22°C. The values are normalized to a spring constant of 1 N/m. A transformation to other spring constants is done by dividing with  $\sqrt{c_{\text{cant}}}$ . <sup>a</sup> From Table 1 in [10].

mode	beam <sup>a</sup>	mode	v-shape
B1	0.577 Å	1	0.558 Å
–	–	2	0.000 Å
B2	0.320 Å	3	0.348 Å
–	–	4	0.000 Å
B3	0.188 Å	5	0.206 Å
B4	0.134 Å	6	0.172 Å
–	–	7	0.000 Å
–	–	8	0.092 Å
–	–	9	0.000 Å
B5	0.104 Å	10	0.144 Å

TABLE III: Thermomechanical noise of the photodiode signal  $\sqrt{\langle S_n^2 \rangle}$  of a beam like [10] and a v-shaped cantilever at 22°C. The values are normalized to a spring constant of 1 N/m. A transformation to other spring constants is done by dividing with  $\sqrt{c_{\text{cant}}}$ . <sup>a</sup> From Table 1 in [10].

The thermomechanical noise as it would be measured in the normal force photodiode signal is listed in Table III. The actual values for cantilevers can be calculated by division with  $\sqrt{c_{\text{cant}}}$ .

Note that there is a deviation of 3.4 % for the thermomechanical noise measured in the photodiode signal for the v-shaped cantilever as compared to the rectangular cantilever beam. Thus, for this type of v-shaped cantilevers, spring constants determined by a naive use of the thermal noise method under the simplifying assumption of a rectangular beam model can be expected to be systematically 7 % too large.

Finally, the limitations of the FEA analysis presented here should be discussed briefly. A deviation of the modal shape of a real cantilever from the theoretic model can be expected from the multilayer structure of the cantilever which consists of a Si<sub>3</sub>N<sub>4</sub> ceramics covered with a reflective gold layer. Due to the metallic coating, the cantilever can be prestressed by the interfacial stress between the

gold and the ceramics. For rectangular cantilevers it was shown that there is a slight deviation of experimentally obtained bending shapes as compared to theoretic ones [29]. A similar result must be expected for v-shaped cantilevers. Thus, a conservative estimate of the relative uncertainty of the tip displacement of  $\delta \langle u_n^2 \rangle = 5\%$  ( $\delta \langle S_n^2 \rangle = 5\%$ ) seems appropriate. However, this estimate attributes only to numerical errors and deviations of the true cantilever geometry from the FEA modelling and does not include additional experimental errors.

#### IV. CONCLUSIONS

In conclusion we have calculated the thermal noise of a v-shaped cantilever (Microlever, Type E, Thermomicroscopes) by means of a finite element analysis. The modal shapes of the first ten eigenmodes are given as well as the numerical constants that are needed for a calibration using the thermal noise method. The results also indicate, that there is a systematic deviation in the thermomechanical noise of v-shaped cantilevers as compared to rectangular beam shaped cantilevers. Thus, when a fast and precise calibration of a v-shaped cantilever is desirable, a numerical modal analysis of the special type of cantilever to be calibrated is inevitable. If the spring constant has to be calibrated with an uncertainty better than 5 % the use of complimentary methods to the thermal noise method is necessary.

#### V. ACKNOWLEDGMENTS

We thank Dr. Heribert Lorenz (Nanotools GmbH) for SEM imaging. Financial support by grant BMBF 13N7509/1 (RWS) and DFG Grant He-1617/7-2 (TD) is gratefully acknowledged.

#### REFERENCES

- [1] D. Smith, Rev. Sci. Instr. **66**(5), 3191 (1995).
- [2] A. García-Valenzuela and J. Villatoro, J. Appl. Phys. **84**(1), 58 (1998).
- [3] F. Gittes and C. Schmidt, Eur. Biophys. J. **27**, 75 (1998).
- [4] P. Saulson, Phys. Rev. D **42**(8), 2437 (1990).
- [5] J. Cleveland, T. Schaffer, and P. Hansma, Phys. Rev. B **52**(12), R8692 (1995).
- [6] A. Roters, M. Gelbert, M. Schimmel, J. Rühle, and D. Johannsmann, Phys. Rev. E **56**(3), 3256 (1997).
- [7] M. Gelbert, A. Roters, M. Schimmel, J. Rühle, and D. Johannsmann, Surf. Interface Anal. **27**, 572 (1999).
- [8] J. Hutter and J. Bechhoefer, Rev. Sci. Instr. **64**(7), 1868 (1993).
- [9] J. Hutter and J. Bechhoefer, Rev. Sci. Instr. **64**(11), 3342 (1993).
- [10] H. Butt and M. Jaschke, Nanotechnology **6**, 1 (1995).
- [11] E. Florin, M. Rief, H. Lehmann, M. Ludwig, C. Dornmair, V. Moy, and H. Gaub, Biosens. Bioelectr. **10**(9-10), 895 (1995).
- [12] D. Walters, J. Cleveland, N. Thomson, P. Hansma, M. Wendman, G. Gurley, and V. Elings, Rev. Sci. Instr. **67**(10), 3583 (1996).
- [13] J. Chon, P. Mulvaney, and J. Sader, J. Appl. Phys. **87**(8), 3978 (2000).
- [14] M. Salapaka, H. Bergh, J. Lai, A. Majumdar, and E. McFarland, J. Appl. Phys. **81**(6), 2480 (1997).
- [15] J. Sader, J. Appl. Phys. **84**(1), 64 (1998).
- [16] W. Han, S. Lindsay, and T. Jing, Appl. Phys. Lett. **69**(26), 4111 (1996).
- [17] H. Schindler, D. Badt, P. Hinterdorfer, F. Kienberger, A. Raab, S. Wielert-Badt, and V. Pastushenko, Ultramicroscopy **82**(1-4), 227 (2000).
- [18] T. Drobek, R. Stark, M. Gräber, and W. Heckl, New J. Phys. **1**, 15.1 (1999).
- [19] R. Stark, T. Drobek, and W. Heckl, Appl. Phys. Lett. **74**(22), 3296 (1999).
- [20] R. Stark and W. Heckl, Surf. Sci. **457**(1-2), 219 (2000).
- [21] S. Thalhammer, R. Stark, S. Müller, J. Wienberg, and W. Heckl, J. Struct. Biol. **119**, 232 (1997).
- [22] R. Stark, S. Thalhammer, J. Wienberg, and W. Heckl, Appl. Phys. A **66**, S579 (1998).
- [23] H. Lang, R. Berger, C. Andreoli, J. Brugger, M. Despont, P. Vettiger, C. Gerber, J. Gimzewski, J. Ramseyer, E. Meyer, and H.-J. Güntherodt, Appl. Phys. Lett. **72**(3), 383 (1998).
- [24] R. Clough and J. Penzien, *Dynamics of structures* (McGraw-Hill, Singapore, 1993), 2nd ed.
- [25] M. Géradin and D. Rixen, *Mechanical vibrations: theory and application to structural dynamics* (Wiley, New York, 1997), 2nd ed.
- [26] *Ansys 5.4* (Ansys Inc., Canonsburg (PA), USA, 1998).
- [27] R. Stark, *Dynamische und quasistatische Rasterkraftmikroskopie zur Materialcharakterisierung: Theorie und Experiment*, Phd thesis, Universität München (2000).
- [28] J. Hazel and V. Tsukruk, Thin Solid Films **339**, 249 (1999).
- [29] U. Rabe, K. Janser, and W. Arnold, Rev. Sci. Instr. **67**(9), 3281 (1996).